Published in final edited form as:

Sci Transl Med. 2025 September 10; 17(815): eadv2106. doi:10.1126/scitranslmed.adv2106.

Impaired TIM4-mediated efferocytosis by liver macrophages contributes to fibrosis in metabolic dysfunction–associated steatohepatitis

Hongxue Shi[1,*], **Xiaobo Wang**[1], **Christopher Sloas**[2], **Brennan Gerlach**[1], **Arif Yurdagul Jr.**[1], **Mary P. Moore**[1], **Eui Jung Jung**[1], **Faridoddin Mirshahi**[3], **Luisa Ronzoni**[4], **Arun J. Sanyal**[3], **Luca Valenti**[4,5], **Chyuan-Sheng Lin**[6], **James Montgomery**[2], **Bradley Zinker**[2], **Michael Klichinsky**[2], **Ira Tabas**[1,6,7,*]

[1] Department of Medicine, Columbia University Irving Medical Center, New York, NY 10032, USA.

[2] Carisma Therapeutics Inc., Philadelphia, PA 19104, USA.

[3] Divsion of Gastroenterology, Hepatology, and Nutrition, Department of Internal Medicine, Virginia Commonwealth University, Richmond, VA 23298, USA.

[4] Precision Medicine Lab, Biological Resource Center, Department of Transfusion Medicine, Fondazione Ca' Granda Ospedale Maggiore Policlinico Milano, Milano 20122, Italy.

[5] Department of Pathophysiology and Transplantation, Universitàdegli Studi di Milano, Milan 20122, Italy.

[6] Department of Pathology and Cell Biology, Columbia University Irving Medical Center, New York, NY 10032, USA.

[7] Department of Physiology and Cellular Biophysics, Columbia University Irving Medical Center, New York, NY 10032, USA.

Abstract

Hepatocyte apoptosis is a key feature of metabolic dysfunction–associated steatohepatitis (MASH), but the fate of apoptotic hepatocytes in MASH is poorly understood. Here, we explore the hypotheses that clearance of dead hepatocytes by liver macrophages (efferocytosis) is impaired in MASH because of low expression of the efferocytosis receptor T cell immunoglobulin and mucin domain containing 4 (TIM4; gene *Timd4*) by MASH liver macrophages, which then

*Corresponding author. hs3205@columbia.edu (H.S.); iat1@columbia.edu (I.T.).

Author contributions: H.S. conducted the mouse experiments, immunofluorescence staining, and data analysis; X.W. carried out mouse injections, immunohistochemistry, H&E and PSR staining, and data collection; C.S. and B.Z. engineered the TIM4 macrophages and their testing ex vivo; B.G. and A.Y. performed the ex vivo primary liver macrophage efferocytosis assays; M.P.M. and E.J.J. isolated mRNA and conducted qPCR assays; H.S., M.K., J.M., and I.T. participated in the design of the macrophage therapy experiments; L.V., A.J.S., and F.M. contributed to the human liver studies; C.-S. L. designed and generated the *Timd4* KD and inducible transgenic models. H.S. and I.T. designed all of the experiments and drafted the manuscript. All authors revised the manuscript and approved the final version.

Competing interests: C.S., J.M., M.K., and B.Z. are employees of Carisma Therapeutics Inc., which has given a research grant to the laboratory of I.T. H.S. and I.T are listed as inventors on a US provisional patent application related to the topic of this study (entitled "Restoring TIM4 in liver macrophages to treat nonalcoholic steatohepatitis (NASH)," USSN: no. 63/584805). All other authors declare that they have no competing interests.

drives liver fibrosis in MASH. We show that apoptotic hepatocytes accumulate in human and experimental MASH, using mice fed the fructose-palmitate-cholesterol (FPC) diet or the high-fat, choline-deficient amino acid–defined (HF-CDAA) diet. Apoptotic hepatocyte accumulation is associated with impaired efferocytosis and loss of TIM4. Administration of neutralizing anti-TIM4 antibodies or genetic deletion of *Timd4* in Kupffer cells of FPC and HF-CDAA diet–fed mice decreased efferocytosis by liver macrophages, increased profibrotic activation of collagen-producing hepatic stellate cells (HSCs), and accelerated the progression to fibrotic MASH. Genetic restoration of macrophage *Timd4* in FPC and HF-CDAA diet–fed MASH mice or cell therapy with $TIM4^+$ macrophages enhanced apoptotic hepatocyte clearance and decreased HSC activation and liver fibrosis. Studies using an ex vivo macrophage HSC cross-talk model and the HF-CDAA MASH model revealed that inactivation of HSCs by efferocytosing macrophages involved macrophage reprogramming to secrete interleukin-10 (IL-10), which activated the IL-10 receptor on HSCs to dampen their profibrotic activation. These findings reveal a key process in the progression from hepatic steatosis to early MASH fibrosis and identify a mechanism-based therapeutic strategy to prevent fibrotic MASH progression.

INTRODUCTION

Metabolic dysfunction–associated steatohepatitis [MASH; formerly nonalcoholic steatohepatitis (NASH)] is emerging as the leading cause of liver disease (1), characterized by hepatosteatosis; inflammation; and, most importantly, liver fibrosis due to activation of hepatic stellate cells (HSCs) (2, 3). However, limited pharmacological therapies exist to mitigate liver fibrosis in MASH (4, 5). An important feature of MASH is hepatocyte death, as well as apoptosis and necroptosis, but the mechanisms linking hepatocyte death with MASH progression, particularly liver fibrosis, remain poorly understood (6, 7). One possibility is that dead hepatocytes release factors that promote HSC activation and liver fibrosis (8–10). However, clinical evidence that blocking caspase-dependent apoptosis mitigates MASH is lacking. For example, the pan-caspase inhibitor emricasan failed to improve liver histology and paradoxically increased liver fibrosis in patients with MASH (11).

The accumulation of dead cells in disease settings indicates impaired clearance of dead cells by macrophages (“efferocytosis”) (12, 13). Macrophages bind apoptotic cells through cell surface receptors, leading to dead cell engulfment and degradation. Efferocytosis not only prevents dead cell accumulation but also reprograms macrophages to execute tissue resolution functions, and impaired efferocytosis contributes to many human chronic inflammatory diseases (12, 13). Accordingly, we hypothesized that the accumulation of dead hepatocytes in MASH reflects impaired efferocytosis and proresolving macrophage reprogramming (14). In a previous study, we showed that the clearance of necroptotic hepatocytes is impaired in MASH, contributing to MASH progression (15), but the mechanism requires further study. Other groups have shown that deletion of triggering receptor expressed on myeloid cells 2 (TREM2) in macrophages impairs efferocytosis ex vivo and exacerbates experimental MASH (16–19) and that TREM2-mediated efferocytosis by liver macrophages can promote the repair of liver injury (20). However, the mechanisms

linking efferocytosis to MASH progression, particularly MASH fibrosis, and the therapeutic implications remain to be fully elucidated.

Previous in vitro studies have shown that T cell immunoglobulin and mucin domain containing 4 (TIM4; gene *Timd4*) can mediate efferocytosis by normal liver resident macrophages [Kupffer cells (KCs)] (21–23), but the role of TIM4 in efferocytosis and liver fibrosis in MASH is unknown. On the basis of these in vitro data and the finding that TIM4 is decreased in MASH liver macrophages compared with KCs (24–27), we hypothesized that loss of TIM4 may impair efferocytosis in MASH and thereby contribute to MASH progression. To test this hypothesis, we used diet-induced mouse MASH models with TIM4 loss of function (neutralization antibody or genetic targeting) or TIM4 gain of function (macrophage-inducible transgenesis).

RESULTS

Efferocytosis by liver macrophages is decreased in human and experimental MASH and is correlated with the loss of macrophage TIM4

Apoptosis in hepatocytes is a key feature of MASH, and accumulation of apoptotic hepatocytes has been reported in MASH liver (6, 7). Given that efferocytosis by macrophages is crucial in clearing dead cells and maintaining tissue homeostasis, we postulated that the efferocytic ability of liver macrophages is impaired in advanced MASH versus early MASH. To evaluate our hypothesis, we used human liver biopsy specimens with various metabolic dysfunction–associated steatotic liver disease activity scores {referred to as NAS [nonalcoholic fatty liver disease (NAFLD) activity score] based on the older term NASH} and conducted an in situ efferocytosis assay, as we previously described (28–30). On the basis of measurements of the ratio of macrophage-associated:free terminal deoxynucleotidyl transferase–mediated deoxyuridine triphosphate nick end labeling$^+$ (TUNEL$^+$) cells, efferocytosis by liver macrophages was markedly decreased in advanced MASH liver (NAS, 3 to 6) compared with normal or early MASH liver (NAS, 0 to 2). In addition, the decrease in efferocytosis in MASH liver was accompanied by an increase in the total number of TUNEL$^+$ cells (Fig. 1A). We next explored a mouse model of steatohepatitis in which mice are fed the high-fat, choline-deficient amino acid–defined (HF-CDAA) diet (31, 32). These mice develop hepatic steatosis at 2 weeks, early liver fibrosis at 4 weeks, and advanced liver fibrosis at 8 and 12 weeks of diet feeding (fig. S1A) (31, 32). Consistent with the human data, the ratio of macrophage-associated:free cl-caspase3$^+$ (apoptotic) cells, which is a measure of efferocytosis by liver macrophages, was markedly decreased at the 8- and 12-week time points, accompanied by an increase in cl-caspase3$^+$ cells (Fig. 1B).

One mechanism of impaired efferocytosis is the loss of macrophage receptors that recognize apoptotic cells. We therefore measured mRNAs encoding efferocytosis receptors in 12-week HF-CDAA–fed mice versus chow-fed mice. The mRNAs encoding *c-mer proto-oncogene tyrosine kinase* (*Mertk*), *brain-specific angiogenesis inhibitor 1* (*Bai1*), and *AXL receptor tyrosine kinase* (*Axl*) were increased, not decreased, in MASH versus control liver (fig. S1B, first three groups), suggesting that defective efferocytosis in MASH cannot be explained by deficiencies in these receptors. The finding with *Mertk* is consistent with our previous

demonstration that liver macrophage efferocytosis in mice fed the MASH-inducing fructose-palmitate-cholesterol (FPC) diet for 16 weeks was not impaired by deletion of macrophage MerTK (33), and we now show similar results using the HD-CDAA MASH model (fig. S1C). However, consistent with previous reports in MASH mice (24–27), the mRNA encoding the efferocytosis receptor TIM4 (*Timd4*) and TIM4 protein were decreased in the livers of both FPC- and HF-CDAA–induced MASH mice (fig. S1B, fourth group, and fig. S1, D to I). We observed a decrease in *Timd4* expression after 8 weeks of HF-CDAA feeding (fig. S1D), which coincides with the point at which impaired liver macrophage efferocytosis occurs in the HF-CDAA model (see Fig. 1B). In addition, both liver TIM4 protein by immunoblot and TIM4 expression in Clec4f$^+$ KCs by immunofluorescence microscopy were decreased after 12 weeks of HF-CDAA feeding (fig. S1, E and F). Similar results were found in the livers of mice fed the FPC MASH diet for 16 weeks (fig. S1, G to I). Consistent with the HF-CDAA time course data above, KC TIM4 expression was not decreased in 8-week FPC-fed mice (fig. S1J), which have steatosis but not MASH (34). TIM4, as measured by immunoblot, was decreased in human MASH liver compared with normal liver (Fig. 1C), and immunofluorescence staining showed that the expression of TIM4 in liver CD68$^+$ macrophages was decreased in human MASH (Fig. 1D). These data are consistent with data in the Gene Expression Omnibus dataset GSE126848 showing that *TIMD4* mRNA is lower in human MASH versus control liver (35). In summary, mouse and human MASH show evidence of impaired efferocytosis, and this is associated with a decrease in TIM4 expression on liver macrophages. On the basis of these findings, we focused on the hypothesis that the decrease in macrophage TIM4 in MASH is a key mechanism for impaired efferocytosis and, consequently, progression to fibrotic MASH.

Antibody-mediated TIM4 blockade and genetic deletion of KC TIM4 reduce efferocytosis and accelerate liver fibrosis in experimental MASH

To investigate the role of TIM4 in the clearance of apoptotic hepatocytes by human KCs ex vivo, we incubated primary human KCs with fluorescently labeled Fas-induced apoptotic hepatocytes in the presence of anti-TIM4 versus immunoglobulin G (IgG) control. Anti-TIM4 decreased efferocytosis as measured by either volume or mean fluorescence intensity (MFI) of engulfed apoptotic hepatocytes (Fig. 2A). Similar results were found using primary mouse liver KCs (Fig. 2B). To evaluate the role of TIM4 in early steatohepatitis, mice were fed the HF-CDAA diet for 4 weeks, with anti-TIM4 or IgG administered during weeks 3 and 4 (Fig. 2C). The two groups of mice had similar body and liver weights (fig. S2A). Anti-TIM4 administration decreased the ratio of macrophage-associated:free cl-caspase3$^+$ (apoptotic) cells, indicating impaired efferocytosis (Fig. 2D). Anti-TIM4 increased liver fibrosis as assessed by both picrosirius red and collagen 1A1 (COL1A1) staining (Fig. 2, E and F). Hepatic stellate cell activation was also increased by anti-TIM4 administration, as indicated by higher α–smooth muscle actin$^+$ (α-SMA$^+$) and osteopontin$^+$ (Opn$^+$) areas (Fig. 2, G and H). The livers of the anti-TIM4 cohort also showed an increased cytokeratin 19$^+$ (CK19$^+$) area, indicating the presence of bile ductular reaction (Fig. 2I), which is associated with MASH pathogenesis (36, 37). Last, anti-TIM4 administration increased the number of hepatic F4/80$^+$ macrophage crown-like structures (hCLS) in the liver (Fig. 2J), which is a characteristic feature of mouse and human MASH associated with liver fibrosis (10). In

contrast, anti-TIM4 did not affect hepatosteatosis, plasma alanine aminotransferase (ALT) activity, or liver macrophage as assessed by *Adgre1* mRNA (fig. S2, B to D).

To investigate the role of KC TIM4 in liver efferocytosis and steatohepatitis progression, we generated *Timd4*$^{fl/fl}$ mice (fig. S2E) and crossed them KC-specific with C-type lectin domain family 4, member f (*Clec4f)-Cre* mice (38) to knock down (KD) TIM4 in KCs (KC-TIM4-KD). *Timd4*$^{fl/fl}$ mice were used as the control mice. We first characterized chow-fed mice and found that liver *Timd4* mRNA expression was decreased in KC-TIM4-KD mice, whereas the liver mRNAs of other efferocytosis receptors were similar between KD and control mice (fig. S2F). Consistent with the *Timd4* data, immunofluorescence analysis showed markedly decreased TIM4 expression in liver macrophages in the KD cohort (fig. S2G), whereas the expression of Clec4f was similar in control and KD livers (fig. S2H). We then fed the mice the HF-CDAA diet for 4 weeks and verified decreased KC-TIM4 in the KD livers (Fig. 3A). We chose 4 weeks because the goal was to test the hypothesis that liver fibrosis would be accelerated if TIM4 were knocked down in KCs during a period when *Timd4* in liver was still expressed (see fig. S1D above). The two cohorts had similar body and liver weights and blood glucose (fig. S2, I and J), but KC-TIM4-KD was associated with defective efferocytosis by liver macrophages, indicated by a reduced ratio of macrophage-associated:free cl-caspase3^{+} cells and increased total cl-caspase3^{+} number per field (Fig. 3B). The KD mice had increased liver fibrosis based on picrosirius red and COL1A1 staining (Fig. 3, C and D) and evidence of increased HSC activation based on higher α-SMA^{+} and Opn^{+} areas (Fig. 3, E and F). As with the anti-TIM4 experiment, the KD mice had increased CK19^{+} area and hCLS (Fig. 3, G and H). These changes occurred despite no change in hepatosteatosis and only a modest decrease in plasma ALT activity (fig. S2, K and L). KC-TIM4-KD also lowered efferocytosis and fibrosis in HF-CDAA–fed female mice without affecting hepatosteatosis (Fig. 3, I to K, and fig. S3, A to E).

We also tested the effect of KC-TIM4-KD in the 16-week FPC MASH model (Fig. 3L). As with the HF-CDAA model, we achieved robust KD of KC-TIM4 (fig. S3J), and there were no substantial differences between the two cohorts in body and liver weight, blood glucose, plasma ALT, and hepatosteatosis (fig. S3, F to I). KC-TIM4-KD caused a decrease in efferocytosis by liver macrophages (Fig. 3M) and increases in liver fibrosis (Fig. 3N and fig. S3K); α-SMA^{+} and Opn^{+} areas (fig. S3, L and M); and mRNAs associated with HSC activation, namely, *collagen type I alpha 1 chain* (*Col1a1*), *collagen type I alpha 2 chain* (*Col1a2*), *collagen type III alpha 1 chain* (*Col3a1*), *secreted phosphoprotein 1* (*Spp1*), and *tissue inhibitor of metalloproteinases 1* (*Timp1*) (Fig. 3O). The livers of the KD mice also had increases in CK19^{+} area (fig. S3N) and hCLS (fig. S3O). In contrast, mRNAs encoding proteins associated with inflammation were similar between the two cohorts (fig. S3P). Thus, when KC-TIM4 is genetically lowered in early MASH, before it is naturally lowered in later MASH, the progression to MASH fibrosis is accelerated.

Macrophage TIM4 restoration after the development of steatosis promotes efferocytosis and suppresses the progression to liver fibrosis in MASH mice

The most important causation question related to TIM4, efferocytosis, and MASH is whether the restoration of macrophage TIM4 during the transition from early to advanced

MASH would dampen the progression to liver fibrosis. To achieve this goal, we created a transgenic (Tg) model in which *Timd4* could be expressed in macrophages in a doxycycline (Dox)–inducible manner (iTg mice). We crossed mice transgenic for TRE (7 $tetO^+$ minimal CMV promoter)–*Timd4*-bGHpA, with macrophage-specific *Cd68rtTA* mice, using mice with TRE-*Timd4*-bGHpa alone and *Cd68rtTA* as controls. The iTg and control mice were fed the HF-CDAA diet for 10 weeks, with Dox administered in the drinking water between weeks 6 and 10 (Fig. 4A). This protocol successfully restored TIM4 in liver macrophages (Fig. 4B), and 93.9 ± 1.0% of the TIM4 signal was in $MAC2^+$ (also known as galectin-3) macrophages versus $MAC2^-$ cells (non-macrophages) in the livers of the iTg mice, similar to endogenous TIM4 in control mice (95.5 ± 0.6% in $MAC2^+$ versus $MAC2^-$ cells). Restoration of macrophage TIM4 did not exert any influence on body weight, liver weight, or blood glucose (fig. S4, A and B). The TIM4-restored mice showed improved efferocytosis (Fig. 4C) and decreased liver fibrosis (Fig. 4, D and E), HSC activation (Fig. 4, F and G), bile ductular reaction (Fig. 4H), and hCLS (Fig. 4I). These improvements occurred without any changes in hepatic steatosis or plasma ALT (fig. S4, C and D).

We then conducted a similar experiment in 16-week FPC-fed mice, intervening with Dox between weeks 9 and 16 so that macrophage TIM4 would be restored during steatosis-to-MASH progression (Fig. 4J), which is the period during TIM4 expression and efferocytosis decrease (above) and liver fibrosis increases (34). The results were similar to those with the HF-CDAA model. There was a restoration of liver macrophage TIM4 in the Dox-treated cohort (Fig. 4K), and 91.6 ± 0.9% of the TIM4 signal was in $MAC2^+$ macrophages versus $MAC2^-$ cells in the livers of the iTg mice, similar to endogenous TIM4 in control mice (95.6 ± 1.2% in $MAC2^+$ versus $MAC2^-$ cells). As in the HF-CDAA model, control and iTg mice had similar body weights, liver weights, blood glucose, hepatic steatosis, and plasma ALT (fig. S4, E to H). Restoration of macrophage TIM4 led to improvements in liver macrophage efferocytosis (Fig. 4L) and decreases in liver fibrosis (Fig. 4M and fig. S4I), α-SMA^+ (Fig. 4N) and OPN^+ areas (fig. S4J), mRNAs associated with HSC activation [*Col1a1*, *Col1a2*, *Col1a3*, *transforming growth factor*–β*1* (*Tgfb1*), and *Timp1*] (Fig. 4O), $CK19^+$ areas (fig. S4K), and hCLS (fig. S4L). In contrast, mRNAs encoding proteins associated with inflammation were similar between the two cohorts (fig. S4M).

As a third model, we restored TIM4 in MASH liver by administering TIM4-expressing "designer" macrophages, made by transducing hematopoietic stem cells with retroviral *Timd4* and then allowing them to differentiate into macrophages (Timd4 macrophages). For this experiment, mice were fed the HF-CDAA diet for 8 weeks, followed by intravenous injection of phosphate-buffered saline (PBS), nontransduced control macrophages, or Timd4 macrophages every 2 weeks for the next 8 weeks while continuing the diet (16 weeks total) (Fig. 5A). We also included a nonsteatohepatitis cohort that was maintained on chow diet for the duration of the experiment with PBS injection. In preliminary experiments, we showed that luciferase-expressing bone marrow–derived macrophages (BMDMs; Luc-Mϕs) injected into HF-CDAA–fed mice localized to the liver (fig. S5A) and that preinjection Timd4 macrophages had increased cell surface TIM4 expression compared with control BMDMs (fig. S5B). The control and Timd4 macrophages injected into the recipient CD45.2 mice were from CD45.1 mice. Consistent with the data in fig. S5A, the livers of the mice treated with control macrophages or Timd4 macrophages showed the presence of

CD45.1$^+$ cells, whereas the livers of the mice injected with PBS showed no CD45.1 staining (fig. S5C). We found that treatment with Timd4 macrophages, which elevated liver TIM4 expression as designed (Fig. 5B), enhanced efferocytosis by liver macrophages (Fig. 5C) and lowered liver fibrosis (Fig. 5D). The mice injected with Timd4 Mϕs also had decreases in COL1A1$^+$, α-SMA$^+$, Opn$^+$ areas (Fig. 5, E to G), and hCLS (fig. S5D) compared with mice injected with control BMDMs or PBS. The protective effects of Timd4 macrophages were not associated with changes in body weight, liver weight, plasma ALT, or hepatic steatosis (fig. S5, E to G). We then conducted a similar experiment in 4-week HF-CDAA–fed mice treated with human monocytes transduced with human *TIMD4* and then allowed to differentiate into macrophages [TIMD4 human monocyte–derived macrophages (HMDMs)]. Control groups included mice injected with control HMDMs and non-MASH chow-fed mice injected with saline vehicle, and all mice were analyzed 2 weeks after injection (Fig. 5H). This experiment required the use of NOD *scid* gamma (NSG) mice to prevent an immune allograft reaction. In preliminary in vitro experiments, we documented elevated TIM4 expression by flow cytometry in TIMD4 versus control HMDMs (fig. S6A) and then showed that TIMD4 HMDMs had enhanced efferocytosis ability compared with control HMDMs or HMDMs transduced with an irrelevant plasmid (fig. S6B). Mice treated with TIMD4 HMDMs had enhanced efferocytosis by liver macrophages (Fig. 5I) and decreased liver fibrosis (Fig. 5J and fig. S6C), α-SMA$^+$ areas (Fig. 5K), Opn$^+$ areas (fig. S6D), and hCLS (fig. S6E) compared with mice treated with control HMDMs or saline, without changes in body weight, liver weight, and hepatic steatosis (fig. S6, F and G). These combined data show that restoration of macrophage TIM4 using in vivo transgenesis or cell therapy with TIM4-expressing macrophages improves efferocytosis and dampens the progression to liver fibrosis.

Efferocytosis by liver macrophages stimulates IL-10 production, which lowers HSC activation

Efferocytosis can reprogram macrophages to a proresolving, disease-suppressing state (12, 39), and thus, we wondered whether this process contributed to the antifibrotic effect seen with restoration of TIM4-mediated efferocytosis in MASH. Among the proresolving molecules known to be induced by efferocytosis is interleukin-10 (IL-10) (30, 40), and previous reports not related to MASH have suggested that IL-10 can lower HSC activation and liver fibrosis (41–43). We therefore considered the hypothesis that TIM4-mediated efferocytosis lowers liver fibrosis by inducing the synthesis and secretion of IL-10 by liver macrophages. To begin, we incubated KCs from normal livers or macrophages from the livers of 4-week HF-CDAA–fed mice (early steatohepatitis) with apoptotic hepatocytes. Note that KCs still populate the liver at this 4-week time point. We found that *Il10* mRNA was induced in both types of macrophages by apoptotic hepatocytes (Fig. 6A). IL-10 protein was also increased in early steatohepatitis macrophages exposed to apoptotic hepatocytes (Fig. 6B). We next probed our hypothesis ex vivo. First, we incubated primary mouse HSCs partially activated by a low concentration of TGF-β1 with recombinant IL-10 plus control IgG or anti–IL-10 receptor (IL-10R). IL-10 lowered the expression of *Col3a1* and actin alpha 2, smooth muscle (*Acta2*) in the HSCs, which was prevented by anti–IL-10R (fig. S7A), indicating that IL-10 can deactivate HSCs in an IL-10R–dependent manner. Next, we incubated early steatohepatitis macrophages with or without apoptotic hepatocytes and

then transferred the conditioned medium (CM) to partially activated HSCs treated with anti–IL-10R antibody or control IgG. The CM of early MASH macrophages further activated the HSCs, as indicated by an increase in *Spp1* and *Timp1* mRNAs, but the increase was lower when the CM came from macrophages incubated with apoptotic hepatocytes (Fig. 6C, bars 1 to 3 in each graph). The ability of CM from macrophages exposed to apoptotic hepatocytes to lower HSC activation was abrogated when the HSCs were treated with anti–IL-10R antibody (Fig. 6C, fourth bar in each graph). To prove the importance of TIM4, we conducted another CM experiment comparing early steatohepatitis macrophages from the livers of wild-type (WT) versus KC-TIM4-KD mice. Apoptotic hepatocyte–exposed WT but not TIM4-KD macrophages secreted IL-10 into the medium (Fig. 6D). As before, the CM of WT macrophages exposed to apoptotic hepatocytes lowered HSC expression of *Spp1 and Timp1*, but this effect was not observed with CM from TIM4-KD macrophages exposed to apoptotic hepatocytes (Fig. 6E). These combined in vitro and ex vivo data are consistent with the hypothesis that efferocytosis lowers HSC activation by inducing IL-10.

We next explored this hypothesis in vivo, first analyzing the livers of the macrophage TIM4-KD and macrophage TIM4-iTg MASH mice described in the previous sections. Consistent with the hypothesis, IL-10 expression was decreased in the livers of TIM4-KD mice (fig. S7B) and increased in the livers of TIM4-iTg mice versus the respective control groups (fig. S7C). In contrast, plasma IL-10 was not elevated in the TIM4-iTg mice (fig. S7D). Similarly, IL-10 expression was increased in the livers, but not plasma, of TIM4 macrophage–treated HF-CDAA mice (fig. S7, E to G). We tested causation by determining whether the liver fibrosis–mitigating effect of macrophage TIM4-iTg could be diminished by administration of anti–IL-10R antibody (Fig. 6F). Consistent with the findings from our previous iTg experiment, the livers of iTg versus control mice in the IgG arm showed decreases in Sirius red staining; percent area of COL1A1, α-SMA, and OPN; and F4/80$^+$ crown-like structures (Fig. 6, G to K, third versus first bars). However, all of these parameters were higher in iTg mice treated with anti–IL-10R versus IgG, negating the liver fibrosis–mitigating effect of boosting macrophage TIM4 expression (Fig. 6, G to K, fourth versus third bars). The detrimental effects of anti–IL-10R were not associated with changes in body weight, liver weight, blood glucose, plasma ALT, or hepatic steatosis (fig. S7, H to K). When considered together with the results of the in vitro and ex vivo experiments above and the prior literature on IL-10 (41–43), these data support the overall concepts that impaired TIM4-mediated efferocytosis promotes the progression to liver fibrosis and that genetic correction of this impairment can lower liver fibrosis through the efferocytosis-induced reprogramming of macrophages to secrete IL-10, which decreases HSC activation (fig. S7L).

DISCUSSION

A key feature of MASH is hepatocyte apoptosis, which correlates with the clinically most important feature of the disease, liver fibrosis (6, 7). Therefore, an important area in MASH research is to understand the fate of apoptotic hepatocytes and how hepatocyte apoptosis might be linked to liver fibrogenesis. Addressing these fundamental issues may suggest new types of strategies to prevent fibrosis progression in MASH. In terms of apoptotic hepatocyte fate, the finding that apoptotic hepatocytes increase in advanced human and

experimental MASH suggests that there is a defect in their clearance. However, previous reports examining this area have not provided direct evidence for impaired engulfment of apoptotic hepatocytes by macrophages in MASH liver, given that they did not report the ratio of macrophage-associated:free apoptotic hepatocytes in situ. The data here show that this ratio is lower in human and mouse steatohepatitis/MASH liver versus control liver, is further lowered by genetic KD of macrophage TIM4, and is improved by macrophage TIM4 restoration. These findings are consistent with previous work showing that TIM4 can function as an efferocytosis receptor (21–23) and that TIM4 expression by liver macrophages is decreased in MASH (24–27). We showed that the changes in TIM4-mediated efferocytosis in our various models were directly and mechanistically linked to liver fibrosis, that is, increased fibrosis with macrophage TIM4 KD and vice versa for macrophage TIM4 restoration. These findings complement those of a previous report from our group examining the fate of hepatocytes that undergo a different type of cell death, necroptosis. We showed that the clearance of necroptotic hepatocytes is also defective in steatohepatitis/MASH, but the mechanism is due to increases in signal regulatory protein alpha (SIRPα) on MASH liver macrophages and CD47 on necroptotic hepatocytes rather than a decrease in a specific macrophage receptor (15). Although blocking either SIRPα or CD47 improved necroptotic hepatocyte uptake and dampened the progression to liver fibrosis, these manipulations did not lower apoptotic hepatocytes (15). We therefore conclude that defective clearance of both necroptotic and apoptotic hepatocytes, which is caused by distinct mechanisms, both contribute to liver fibrosis in steatohepatitis/MASH.

A question that we have begun to address in this study is the mechanism linking defective clearance of apoptotic hepatocytes in MASH to liver fibrosis. In theory, the accumulation of apoptotic hepatocytes could directly contribute to fibrosis, for example, by releasing fibrogenic factors (8, 9, 37). However, the failure of apoptosis inhibitors to block MASH fibrosis in humans (11) suggests the possibility of alternative mechanisms. In this context, efferocytosis reprograms macrophages to carry out tissue resolution, and one such efferocytosis-induced resolution program that attracted our attention was the induction and secretion of IL-10. Efferocytosis leads to IL-10 induction in macrophages through signaling pathways activated by apoptotic cell cargo, including fatty acids and tryptophan (30, 40). Previous work has shown that transgenic overexpression of IL-10 or IL-10 administration in mice reduced carbon tetrachloride–induced liver fibrosis, which was linked to decreased HSC activation ascribed to various mechanisms, including a decrease in $CD4^+$ T cells and induction of HSC senescence (41–43). Moreover, in mice exposed to carbon tetrachloride or acetaminophen, signal transducer and activator of transcription 3–IL-10–IL-6–induced reprogramming of efferocytosing macrophages contributed to liver repair (44). Our combined ex vivo macrophage HSC cross-talk data and in vivo MASH causation data support the idea that IL-10 is an important link between TIM4-mediated efferocytosis and protection from fibrosis in MASH. However, it is possible that efferocytosis induces the secretion of other antifibrotic factors or suppresses profibrotic factors in liver macrophages. In addition to the loss of macrophage-secreted IL-10 and possibly other macrophage-mediated MASH-protective mechanisms, impaired efferocytosis may also lead to additional profibrotic processes, such as HSC activation by uncleared dead hepatocytes. Another efferocytosis receptor, TREM2, undergoes cleavage in MASH (16), and genetic deletion

of *Trem2* in mice is associated with MASH progression (16–19). However, whether TREM2 cleavage directly promotes MASH progression and, if so, whether the mechanism is related to impaired efferocytosis and IL-10 production remain to be explored. Last, an interesting aspect related to efferocytosis-induced macrophage reprogramming in MASH is that efferocytosis in other settings can promote fibrosis as part of the tissue resolution process, for example, by secreting TGF-β1 (12, 13). Thus, we propose that this reprogramming process has some distinct features in the unique setting of MASH, which is consistent with our showing that restoration of TIM4-mediated efferocytosis in MASH decreased liver *Tgfb1*. One factor may be the type of engulfed apoptotic cell, given that a previous study showed that the uptake of apoptotic hepatocytes by IL-4–treated BMDMs in vitro promotes an immune-suppressive phenotype (45), whereas another study showed that the uptake of apoptotic neutrophils by liver macrophages in the setting of carbon tetrachloride (CCl_4)–induced liver injury promotes TGF-β1–mediated HSC activation (46). Further studies will be needed to further investigate this topic.

Previous preclinical studies have shown that macrophage therapy can reduce carbon tetrachloride–induced liver fibrosis (47–50) or promote the repair of acute liver injury repair (44, 51). Moreover, recent clinical trials have provided evidence that the administration of autologous macrophage therapy for liver fibrosis is safe, although the nature of these trials precluded efficacy assessment (52, 53). We reason that the insights gained from this study could lead to previously unknown therapeutic strategies for improving liver fibrosis, which is the most important yet challenging aspect of MASH. By way of illustration, we conducted a proof-of-concept experiment showing the benefit of cell therapy using TIM4-expressing macrophages. Future iterations could involve administering macrophages expressing highly functional chimeric efferocytosis receptors (54), delivering mRNA (or small interfering RNA) to macrophages in vivo to boost efferocytosis (55), and using macrophage or RNA therapy that targets more than one MASH fibrosis mechanism. For example, the MASH fibrosis–protective mechanisms of boosting apoptotic hepatocyte clearance (here) and necroptotic hepatocyte clearance (15) are distinct and complementary, suggesting a possible additive benefit of enhancing both processes by combination cell or RNA therapy. Last, fibrotic MASH is an independent risk factor for atherosclerotic cardiovascular disease, which is the leading cause of death in people with MASH (56). Moreover, defective macrophage efferocytosis drives the formation of clinically dangerous (“unstable”) atherosclerotic plaques (57). Thus, efferocytosis-promoting therapy might lower cardiovascular risk in MASH subjects by dual mechanisms, that is, by decreasing liver fibrosis and directly improving plaque stability.

We note several limitations of this study. First, experimental MASH models may not reflect human MASH both in terms of mechanisms and treatment strategies. We attempted to mitigate this limitation by using complementary mouse models, each of which shares features with human MASH, and by looking for key aspects of our discoveries in human MASH liver and primary liver cells from human liver. Second, the exact molecular genetic mechanism through which the uptake of apoptotic hepatocytes reprograms macrophages to synthesize and secrete IL-10 remains to be elucidated. Third, scalability issues would make repeated macrophage therapy a challenging approach to treating a chronic disease such as

MASH. However, as noted above, the overall concept of this approach could be applied to efferocytosis enhancement treatments that are much more scalable, such as mRNA therapy.

In summary, we have shown that decreased expression of TIM4 in liver macrophages during MASH progression contributes to defective efferocytosis, leading to impaired macrophage IL-10 production and increased HSC activation and liver fibrosis. Accordingly, genetic restoration of TIM4 in macrophages in MASH or treatment of MASH mice with macrophages genetically engineered to express TIM4 improves the clearance of apoptotic hepatocytes and decreases liver fibrosis. These findings elucidate a key mechanism of impaired efferocytosis in MASH, provide insight into how impaired efferocytosis activates HSCs in MASH, and suggest how this knowledge can be used to design previously unknown therapeutic strategies to block MASH fibrosis.

MATERIALS AND METHODS

Study design

The objective was to test the hypothesis that decreased expression of the efferocytosis receptor TIM4 in liver macrophages causes impaired clearance of apoptotic hepatocytes by liver macrophages, which promotes the progression to fibrotic MASH. We first compared human and mouse normal versus MASH livers for apoptotic hepatocytes, macrophage TIM4 expression, and in situ efferocytosis. We then treated primary human and mouse KCs with anti-TIM4 antibody or siTimd4 and assayed the uptake of apoptotic hepatocytes. Next, we tested in vivo whether anti-TIM4 or genetic deletion of TIM4 in KCs could accelerate liver fibrosis in two validated models of diet-induced MASH/steatohepatitis models, the FPC model and the HF-CDAA model. Conversely, we tested whether inducible restoration of TIM4 in macrophages in mice with steatohepatitis or treatment of steatohepatitis with macrophages genetically engineered to overexpress TIM4 could restore efferocytosis and dampen MASH fibrosis. Last, we tested the hypothesis ex vivo and in steatohepatitis mice that efferocytosis-induced IL-10, by interacting with the IL-10 receptor on HSCs, could lower HSC activation and thereby lower liver fibrosis. The ex vivo experiments were repeated with at least three biological replicates, and the in vivo experiments used $n > 7$ mice per group and two complementary diet–induced MASH/steatohepatitis models. The sample size for the mouse experiments was determined by previous mouse MASH or pilot experiments. Data exclusion criteria in the mouse experiments were >20% loss of body weight during the diet feeding period or a ratio of liver weight to body weight of <6% after MASH diet feeding. All mouse experiments were approved by the Columbia University Institutional Animal Care and Use Committee (protocol no. AABL5573). The data were analyzed in an unblinded manner. Human studies were approved by Columbia University Institutional Review Board (protocol no. IRB-AAAU1906).

Animal studies

Male WT C57/BL6J mice (10 to 12 weeks old, no. 000664) were obtained from the Jackson Laboratory and were allowed to adjust to the housing environment in the Columbia University Irving Medical Center for 1 week before starting experiments. The mice were fed an FPC diet (Envigo, no. TD. 160785 PWD) for 8 or 16 weeks to develop simple

steatosis and fibrotic MASH, respectively (34), or an HF-CDAA diet (Research Diets, no. A06071302) for 4 or 10 weeks to induce early or advanced steatohepatitis, respectively (31). Age-matched male mice were fed a control diet (PicoLab Rodent Diet 20, no. 5053). All of the mice were randomly assigned to experimental groups by investigators who were blinded in terms of group assignment. All mice were housed in standard cages at 22°C in a 12:12-hour light-dark cycle in a barrier facility, and experiments were conducted by following the *Guidelines for the Care and Use of Laboratory Animals* at Columbia University. Animal protocol AABL5573 for these studies was approved by the Institutional Animal Care and Use Committee at Columbia University.

Statistical analysis

All quantitative data are presented as mean ± SEM. Statistical significance was determined using GraphPad Prism software (version 9.3). The Shapiro-Wilk test was used to test normality. Statistical significance between two groups was analyzed using the Student's *t* test, and multiple groups were analyzed using one-way or two-way analysis of variance (ANOVA) with Fisher's least significant difference (LSD) post hoc analysis. *P* values less than 0.05 were considered statistically significant.

Supplementary Material

Refer to Web version on PubMed Central for supplementary material.

Acknowledgments:

We thank D. Ngai and M. Schilperoort (CUIMC) for manuscript editing and R. Schwabe (CUIMC) for helpful discussions. The schematic summary in Fig. 6L was created with BioRender.com.

Funding:

This work was supported by NIH grants K99DK137021 to H.S. and R01DK116620 and R01DK133694 to I.T.; an American Liver Foundation Liver Scholar Award to X.W.; and a grant from the Ines Mandl Research Foundation to M.P.M. Samples for histological analysis were prepared in the Molecular Pathology Shared Resource of the Herbert Irving Comprehensive Cancer Center at Columbia University, supported by NIH/NCI (National Cancer Institute) grant no. P30 CA 013696. Immunofluorescent imaging experiments were conducted in the Columbia Center for Translational Immunology Core Facility, funded by NIH grants P30CA 013696, S10RR027050, and S10OD020056. The Genetically Modified Mouse Models Shared Resource at Columbia is supported partially by P30CA 013696. Normal and MASH human livers were obtained through the Liver Tissue Delivery System, Minneapolis, Minnesota, which was funded by NIH contract no. 75N94022P00816.

Data and materials availability:

All data associated with this study are present in the paper or the Supplementary Materials. Primary data are available in data file S1. All materials are available upon request, with material transfer agreement required for *Timd4* KD and inducible transgenic mice.

REFERENCES AND NOTES

1. Younossi ZM, Paik JM, Henry L, Yang J, Fernandes G, Stepanova M, Nader F, The growing economic and clinical burden of nonalcoholic steatohepatitis (NASH) in the United States. J. Clin. Exp. Hepatol. 13, 454–467 (2023). [PubMed: 37250870]
2. Loomba R, Friedman SL, Shulman GI, Mechanisms and disease consequences of nonalcoholic fatty liver disease. Cell 184, 2537–2564 (2021). [PubMed: 33989548]

3. Tacke F, Weiskirchen R, Non-alcoholic fatty liver disease (NAFLD)/non-alcoholic steatohepatitis (NASH)-related liver fibrosis: Mechanisms, treatment and prevention. Ann. Transl. Med. 9, 729 (2021). [PubMed: 33987427]

4. Harrison SA, Allen AM, Dubourg J, Noureddin M, Alkhouri N, Challenges and opportunities in NASH drug development. Nat. Med. 29, 562–573 (2023). [PubMed: 36894650]

5. Harrison SA, Bedossa P, Guy CD, Schattenberg JM, Loomba R, Taub R, Labriola D, Moussa SE, Neff GW, Rinella ME, Anstee QM, Abdelmalek MF, Younossi Z, Baum SJ, Francque S, Charlton MR, Newsome PN, Lanthier N, Schiefke I, Mangia A, Pericàs JM, Patil R, Sanyal AJ, Noureddin M, Bansal MB, Alkhouri N, Castera L, Rudraraju M, Ratziu V, A phase 3, randomized, controlled trial of resmetirom in NASH with liver fibrosis. N. Engl. J. Med. 390, 497–509 (2024). [PubMed: 38324483]

6. Schwabe RF, Luedde T, Apoptosis and necroptosis in the liver: A matter of life and death. Nat. Rev. Gastroenterol. Hepatol. 15, 738–752 (2018). [PubMed: 30250076]

7. Feldstein AE, Canbay A, Angulo P, Taniai M, Burgart LJ, Lindor KD, Gores GJ, Hepatocyte apoptosis and fas expression are prominent features of human nonalcoholic steatohepatitis. Gastroenterology 125, 437–443 (2003). [PubMed: 12891546]

8. Zhang B, Lapenta K, Wang Q, Nam JH, Chung D, Robert ME, Nathanson MH, Yang X, Trefoil factor 2 secreted from damaged hepatocytes activates hepatic stellate cells to induce fibrogenesis. J. Biol. Chem. 297, 100887 (2021). [PubMed: 34146542]

9. Mederacke I, Filliol A, Affo S, Nair A, Hernandez C, Sun Q, Hamberger F, Brundu F, Chen Y, Ravichandra A, Huebener P, Anke H, Shi H, Martínez García de la Torre RA, Smith JR, Henderson NC, Vondran FWR, Rothlin CV, Baehre H, Tabas I, Sancho-Bru P, Schwabe RF, The purinergic P2Y14 receptor links hepatocyte death to hepatic stellate cell activation and fibrogenesis in the liver. Sci. Transl. Med. 14, eabe5795 (2022). [PubMed: 35385339]

10. Itoh M, Kato H, Suganami T, Konuma K, Marumoto Y, Terai S, Sakugawa H, Kanai S, Hamaguchi M, Fukaishi T, Aoe S, Akiyoshi K, Komohara Y, Takeya M, Sakaida I, Ogawa Y, Hepatic crown-like structure: A unique histological feature in non-alcoholic steatohepatitis in mice and humans. PLOS ONE 8, e82163 (2013). [PubMed: 24349208]

11. Harrison SA, Goodman Z, Jabbar A, Vemulapalli R, Younes ZH, Freilich B, Sheikh MY, Schattenberg JM, Kayali Z, Zivony A, Sheikh A, Garcia-Samaniego J, Satapathy SK, Therapondos G, Mena E, Schuppan D, Robinson J, Chan JL, Hagerty DT, Sanyal AJ, A randomized, placebo-controlled trial of emricasan in patients with NASH and F1-F3 fibrosis. J. Hepatol. 72, 816–827 (2020). [PubMed: 31887369]

12. Doran AC, Yurdagul A Jr., Tabas I, Efferocytosis in health and disease. Nat. Rev. Immunol. 20, 254–267 (2020). [PubMed: 31822793]

13. Mehrotra P, Ravichandran KS, Drugging the efferocytosis process: Concepts and opportunities. Nat. Rev. Drug Discov. 21, 601–620 (2022). [PubMed: 35650427]

14. Shi H, Moore MP, Wang X, Tabas I, Efferocytosis in liver disease. JHEP Rep. 6, 100960 (2024). [PubMed: 38234410]

15. Shi H, Wang X, Li F, Gerlach BD, Yurdagul A Jr., Moore MP, Zeldin S, Zhang H, Cai B, Zheng Z, Valenti L, Tabas I, CD47-SIRPα axis blockade in NASH promotes necroptotic hepatocyte clearance by liver macrophages and decreases hepatic fibrosis. Sci. Transl. Med. 14, eabp8309 (2022). [PubMed: 36417485]

16. Wang X, He Q, Zhou C, Xu Y, Liu D, Fujiwara N, Kubota N, Click A, Henderson P, Vancil J, Marquez CA, Gunasekaran G, Schwartz ME, Tabrizian P, Sarpel U, Fiel MI, Diao Y, Sun B, Hoshida Y, Liang S, Zhong Z, Prolonged hypernutrition impairs TREM2-dependent efferocytosis to license chronic liver inflammation and NASH development. Immunity 56, 58–77.e11 (2023). [PubMed: 36521495]

17. Liebold I, Meyer S, Heine M, Kuhl A, Witt J, Eissing L, Fischer AW, Koop AC, Kluwe J, Wiesch JSZ, Wehmeyer M, Knippschild U, Scheja L, Heeren J, Bosurgi L, Worthmann A, TREM2 regulates the removal of apoptotic cells and inflammatory processes during the progression of NAFLD. Cells 12, 341 (2023). [PubMed: 36766683]

18. Hendrikx T, Porsch F, Kiss MG, Rajcic D, Papac-Milicevic N, Hoebinger C, Goederle L, Hladik A, Shaw LE, Horstmann H, Knapp S, Derdak S, Bilban M, Heintz L, Krawczyk M, Paternostro R, Trauner M, Farlik M, Wolf D, Binder CJ, Soluble TREM2 levels reflect the recruitment and

expansion of TREM2^{+} macrophages that localize to fibrotic areas and limit NASH. J. Hepatol. 77, 1373–1385 (2022). [PubMed: 35750138]

19. Hou J, Zhang J, Cui P, Zhou Y, Liu C, Wu X, Ji Y, Wang S, Cheng B, Ye H, Shu L, Zhang K, Wang D, Xu J, Shu Q, Colonna M, Fang X, TREM2 sustains macrophage-hepatocyte metabolic coordination in nonalcoholic fatty liver disease and sepsis. J. Clin. Invest. 131, e135197 (2021). [PubMed: 33586673]
20. De Ponti FF, Bujko A, Liu Z, Collins PJ, Schuermans S, Maueroder C, Amstelveen S, Thoné T, Martens L, McKendrick JG, Louwe PA, Sànchez Cruz A, Saelens W, Matchett KP, Waller KJ, Zwicker C, Buglar-Lamb A, Vanneste B, Parmentier F, Binte Abdul Latib M, Remmerie A, Kertesz L, Kremer A, Verbeke J, Ipsen DH, Pfister DR, Liu Z, Guilliams M, Henderson NC, Ravichandran K, Marques PE, Scott CL, Spatially restricted and ontogenically distinct hepatic macrophages are required for tissue repair. Immunity 58, 362–380.e10 (2025). [PubMed: 39862865]
21. Yanagihashi Y, Segawa K, Maeda R, Nabeshima YI, Nagata S, Mouse macrophages show different requirements for phosphatidylserine receptor Tim4 in efferocytosis. Proc. Natl. Acad. Sci. U.S.A. 114, 8800–8805 (2017). [PubMed: 28768810]
22. Miyanishi M, Tada K, Koike M, Uchiyama Y, Kitamura T, Nagata S, Identification of Tim4 as a phosphatidylserine receptor. Nature 450, 435–439 (2007). [PubMed: 17960135]
23. Ni M, Zhang J, Sosa R, Zhang H, Wang H, Jin D, Crowley K, Naini B, Reed FE, Busuttil RW, Kupiec-Weglinski JW, Wang X, Zhai Y, T-cell immunoglobulin and mucin domain-containing protein-4 is critical for Kupffer Cell homeostatic function in the activation and resolution of liver ischemia reperfusion injury. Hepatology 74, 2118–2132 (2021). [PubMed: 33999437]
24. Seidman JS, Troutman TD, Sakai M, Gola A, Spann NJ, Bennett H, Bruni CM, Ouyang Z, Li RZ, Sun X, Vu BT, Pasillas MP, Ego KM, Gosselin D, Link VM, Chong LW, Evans RM, Thompson BM, McDonald JG, Hosseini M, Witztum JL, Germain RN, Glass CK, Niche-specific reprogramming of epigenetic landscapes drives myeloid cell diversity in nonalcoholic steatohepatitis. Immunity 52, 1057–1074.e7 (2020). [PubMed: 32362324]
25. Lefere S, Degroote H, Van Vlierberghe H, Devisscher L, Unveiling the depletion of Kupffer cells in experimental hepatocarcinogenesis through liver macrophage subtype-specific markers. J. Hepatol. 71, 631–633 (2019). [PubMed: 31213365]
26. Tran S, Baba I, Poupel L, Dussaud S, Moreau M, Gélineau A, Marcelin G, Magréau-Davy E, Ouhachi M, Lesnik P, Boissonnas A, Le Goff W, Clausen BE, Yvan-Charvet L, Sennlaub F, Huby T, Gautier EL, Impaired Kupffer cell self-renewal alters the liver response to lipid overload during non-alcoholic steatohepatitis. Immunity 53, 627–640.e5 (2020). [PubMed: 32562600]
27. Daemen S, Gainullina A, Kalugotla G, He L, Chan MM, Beals JW, Liss KH, Klein S, Feldstein AE, Finck BN, Artyomov MN, Schilling JD, Dynamic shifts in the composition of resident and recruited macrophages influence tissue remodeling in NASH. Cell Rep. 34, 108626 (2021). [PubMed: 33440159]
28. Thorp E, Cui D, Schrijvers DM, Kuriakose G, Tabas I, Mertk receptor mutation reduces efferocytosis efficiency and promotes apoptotic cell accumulation and plaque necrosis in atherosclerotic lesions of Apoe$^{-/-}$ mice. Arterioscler. Thromb. Vasc. Biol. 28, 1421–1428 (2008). [PubMed: 18451332]
29. Yurdagul A Jr., Subramanian M, Wang X, Crown SB, Ilkayeva OR, Darville L, Kolluru GK, Rymond CC, Gerlach BD, Zheng Z, Kuriakose G, Kevil CG, Koomen JM, Cleveland JL, Muoio DM, Tabas I, Macrophage metabolism of apoptotic cell-derived arginine promotes continual efferocytosis and resolution of injury. Cell Metab. 31, 518–533.e10 (2020). [PubMed: 32004476]
30. Sukka SR, Ampomah PB, Darville LNF, Ngai D, Wang X, Kuriakose G, Xiao Y, Shi J, Koomen JM, McCusker RH, Tabas I, Efferocytosis drives a tryptophan metabolism pathway in macrophages to promote tissue resolution. Nat. Metab. 6, 1736–1755 (2024). [PubMed: 39242914]
31. Wei G, An P, Vaid KA, Nasser I, Huang P, Tan L, Zhao S, Schuppan D, Popov YV, Comparison of murine steatohepatitis models identifies a dietary intervention with robust fibrosis, ductular reaction, and rapid progression to cirrhosis and cancer. Am. J. Physiol. Gastrointest. Liver Physiol. 318, G174–g188 (2020). [PubMed: 31630534]
32. Vacca M, Kamzolas I, Harder LM, Oakley F, Trautwein C, Hatting M, Ross T, Bernardo B, Oldenburger A, Hjuler ST, Ksiazek I, Lindén D, Schuppan D, Rodriguez-Cuenca S, Tonini MM,

Castañeda TR, Kannt A, Rodrigues CMP, Cockell S, Govaere O, Daly AK, Allison M, Honnens de Lichtenberg K, Kim YO, Lindblom A, Oldham S, Andréasson AC, Schlerman F, Marioneaux J, Sanyal A, Afonso MB, Younes R, Amano Y, Friedman SL, Wang S, Bhattacharya D, Simon E, Paradis V, Burt A, Grypari IM, Davies S, Driessen A, Yashiro H, Pors S, Worm Andersen M, Feigh M, Yunis C, Bedossa P, Stewart M, Cater HL, Wells S, Schattenberg JM, Anstee QM, Tiniakos D, Perfield JW, Petsalaki E, Davidsen P, Vidal-Puig A, An unbiased ranking of murine dietary models based on their proximity to human metabolic dysfunction-associated steatotic liver disease (MASLD). Nat. Metab. 6, 1178–1196 (2024). [PubMed: 38867022]

33. Cai B, Dongiovanni P, Corey KE, Wang X, Shmarakov IO, Zheng Z, Kasikara C, Davra V, Meroni M, Chung RT, Rothlin CV, Schwabe RF, Blaner WS, Birge RB, Valenti L, Tabas I, Macrophage MerTK promotes liver fibrosis in nonalcoholic steatohepatitis. Cell Metab. 31, 406–421.e7 (2020). [PubMed: 31839486]
34. Wang X, Zheng Z, Caviglia JM, Corey KE, Herfel TM, Cai B, Masia R, Chung RT, Lefkowitch JH, Schwabe RF, Tabas I, Hepatocyte TAZ/WWTR1 promotes inflammation and fibrosis in nonalcoholic steatohepatitis. Cell Metab. 24, 848–862 (2016). [PubMed: 28068223]
35. Cao C, Liu W, Guo X, Weng S, Chen Y, Luo Y, Wang S, Zhu B, Liu Y, Peng D, Identification and validation of efferocytosis-related biomarkers for the diagnosis of metabolic dysfunction-associated steatohepatitis based on bioinformatics analysis and machine learning. Front. Immunol. 15, 1460431 (2024). [PubMed: 39497821]
36. Zhao L, Westerhoff M, Pai RK, Choi W-T, Gao Z-H, Hart J, Centrilobular ductular reaction correlates with fibrosis stage and fibrosis progression in non-alcoholic steatohepatitis. Mod. Pathol. 31, 150–159 (2018). [PubMed: 28862262]
37. Lee SJ, Park JB, Kim KH, Lee WR, Kim JY, An HJ, Park KK, Immunohistochemical study for the origin of ductular reaction in chronic liver disease. Int. J. Clin. Exp. Pathol. 7, 4076–4085 (2014). [PubMed: 25120786]
38. Sakai M, Troutman TD, Seidman JS, Ouyang Z, Spann NJ, Abe Y, Ego KM, Bruni CM, Deng Z, Schlachetzki JCM, Nott A, Bennett H, Chang J, Vu BT, Pasillas MP, Link VM, Texari L, Heinz S, Thompson BM, McDonald JG, Geissmann F, Glass CK, Liver-derived signals sequentially reprogram myeloid enhancers to initiate and maintain kupffer cell identity. Immunity 51, 655–670.e8 (2019). [PubMed: 31587991]
39. Morioka S, Maueroder C, Ravichandran KS, Living on the edge: Efferocytosis at the interface of homeostasis and pathology. Immunity 50, 1149–1162 (2019). [PubMed: 31117011]
40. Zhang S, Weinberg S, DeBerge M, Gainullina A, Schipma M, Kinchen JM, Ben-Sahra I, Gius DR, Yvan-Charvet L, Chandel NS, Schumacker PT, Thorp EB, Efferocytosis fuels requirements of fatty acid oxidation and the electron transport chain to polarize macrophages for tissue repair. Cell Metab. 29, 443–456.e5 (2019). [PubMed: 30595481]
41. Safadi R, Ohta M, Alvarez CE, Fiel MI, Bansal M, Mehal WZ, Friedman SL, Immune stimulation of hepatic fibrogenesis by CD8 cells and attenuation by transgenic interleukin-10 from hepatocytes. Gastroenterology 127, 870–882 (2004). [PubMed: 15362042]
42. Zhang LJ, Zheng WD, Chen YX, Huang YH, Chen ZX, Zhang SJ, Shi MN, Wang XZ, Antifibrotic effects of interleukin-10 on experimental hepatic fibrosis. Hepatogastroenterology 54, 2092–2098 (2007). [PubMed: 18251166]
43. Huang YH, Chen MH, Guo QL, Chen ZX, Chen QD, Wang XZ, Interleukin-10 induces senescence of activated hepatic stellate cells via STAT3-p53 pathway to attenuate liver fibrosis. Cell. Signal. 66, 109445 (2020). [PubMed: 31730896]
44. Campana L, Starkey Lewis PJ, Pellicoro A, Aucott RL, Man J, O'Duibhir E, Mok SE, Ferreira-Gonzalez S, Livingstone E, Greenhalgh SN, Hull KL, Kendall TJ, Vernimmen D, Henderson NC, Boulter L, Gregory CD, Feng Y, Anderton SM, Forbes SJ, Iredale JP, The STAT3-IL-10-IL-6 pathway is a novel regulator of macrophage efferocytosis and phenotypic conversion in sterile liver injury. J. Immunol. 200, 1169–1187 (2018). [PubMed: 29263216]
45. Liebold I, Al Jawazneh A, Casar C, Lanzloth C, Leyk S, Hamley M, Wong MN, Kylies D, Gräfe SK, Edenhofer I, Aranda-Pardos I, Kriwet M, Haas H, Krause J, Hadjilaou A, Schromm AB, Richardt U, Eggert P, Tappe D, Weidemann SA, Ghosh S, Krebs CF, A-Gonzalez N, Worthmann A, Lohse AW, Huber S, Rothlin CV, Puelles VG, Jacobs T, Gagliani N, Bosurgi L, Apoptotic

cell identity induces distinct functional responses to IL-4 in efferocytic macrophages. Science 384, eabo7027 (2024). [PubMed: 38574142]

46. Kim KH, Cheng N, Lau LF, Cellular communication network factor 1-stimulated liver macrophage efferocytosis drives hepatic stellate cell activation and liver fibrosis. Hepatol. Commun. 6, 2798–2811 (2022). [PubMed: 35929736]
47. Thomas JA, Pope C, Wojtacha D, Robson AJ, Gordon-Walker TT, Hartland S, Ramachandran P, Van Deemter M, Hume DA, Iredale JP, Forbes SJ, Macrophage therapy for murine liver fibrosis recruits host effector cells improving fibrosis, regeneration, and function. Hepatology 53, 2003–2015 (2011). [PubMed: 21433043]
48. Ma PF, Gao CC, Yi J, Zhao JL, Liang SQ, Zhao Y, Ye YC, Bai J, Zheng QJ, Dou KF, Han H, Qin HY, Cytotherapy with M1-polarized macrophages ameliorates liver fibrosis by modulating immune microenvironment in mice. J. Hepatol. 67, 770–779 (2017). [PubMed: 28596109]
49. Watanabe Y, Tsuchiya A, Seino S, Kawata Y, Kojima Y, Ikarashi S, Starkey Lewis PJ, Lu WY, Kikuta J, Kawai H, Yamagiwa S, Forbes SJ, Ishii M, Terai S, Mesenchymal stem cells and induced bone marrow-derived macrophages synergistically improve liver fibrosis in mice. Stem Cells Transl. Med. 8, 271–284 (2019). [PubMed: 30394698]
50. Dai H, Zhu C, Huai Q, Xu W, Zhu J, Zhang X, Zhang X, Sun B, Xu H, Zheng M, Li X, Wang H, Chimeric antigen receptor-modified macrophages ameliorate liver fibrosis in preclinical models. J. Hepatol. 80, 913–927 (2024). [PubMed: 38340812]
51. Igarashi Y, Wada H, Muto M, Sone R, Hasegawa Y, Seino KI, Amelioration of liver fibrosis with autologous macrophages induced by IL-34-based condition. Inflamm. Regen. 45, 2 (2025). [PubMed: 39856797]
52. Moroni F, Dwyer BJ, Graham C, Pass C, Bailey L, Ritchie L, Mitchell D, Glover A, Laurie A, Doig S, Hargreaves E, Fraser AR, Turner ML, Campbell JDM, McGowan NWA, Barry J, Moore JK, Hayes PC, Leeming DJ, Nielsen MJ, Musa K, Fallowfield JA, Forbes SJ, Safety profile of autologous macrophage therapy for liver cirrhosis. Nat. Med. 25, 1560–1565 (2019). [PubMed: 31591593]
53. Brennan PN, MacMillan M, Manship T, Moroni F, Glover A, Troland D, MacPherson I, Graham C, Aird R, Semple SIK, Morris DM, Fraser AR, Pass C, McGowan NWA, Turner ML, Manson L, Lachlan NJ, Dillon JF, Kilpatrick AM, Campbell JDM, Fallowfield JA, Forbes SJ, Autologous macrophage therapy for liver cirrhosis: A phase 2 open-label randomized controlled trial. Nat. Med. 31, 979–987 (2025). [PubMed: 39794616]
54. Morioka S, Kajioka D, Yamaoka Y, Ellison RM, Tufan T, Werkman IL, Tanaka S, Barron B, Ito ST, Kucenas S, Okusa MD, Ravichandran KS, Chimeric efferocytic receptors improve apoptotic cell clearance and alleviate inflammation. Cell 185, 4887–4903.e17 (2022). [PubMed: 36563662]
55. Wang C, Zhang Y, Dong Y, Lipid nanoparticle-mRNA formulations for therapeutic applications. Acc. Chem. Res. 54, 4283–4293 (2021). [PubMed: 34793124]
56. Finney AC, Das S, Kumar D, McKinney MP, Cai B, Yurdagul A Jr., O. Rom, The interplay between nonalcoholic fatty liver disease and atherosclerotic cardiovascular disease. Front. Cardiovasc. Med. 10, 1116861 (2023). [PubMed: 37200978]
57. Yurdagul A Jr., Doran AC, Cai B, Fredman G, Tabas IA, Mechanisms and consequences of defective efferocytosis in atherosclerosis. Front. Cardiovasc. Med. 4, 86 (2018). [PubMed: 29379788]
58. Kitamura T, Koshino Y, Shibata F, Oki T, Nakajima H, Nosaka T, Kumagai H, Retrovirus-mediated gene transfer and expression cloning: Powerful tools in functional genomics. Exp. Hematol. 31, 1007–1014 (2003). [PubMed: 14585362]
59. Zhang X, Goncalves R, Mosser DM, The isolation and characterization of murine macrophages. Curr. Protoc. Immunol. 14, 14.11.11–14.11.14 (2008).
60. Bobadilla S, Sunseri N, Landau NR, Efficient transduction of myeloid cells by an HIV-1-derived lentiviral vector that packages the Vpx accessory protein. Gene Ther. 20, 514–520 (2013). [PubMed: 22895508]
61. Klichinsky M, Ruella M, Shestova O, Lu XM, Best A, Zeeman M, Schmierer M, Gabrusiewicz K, Anderson NR, Petty NE, Cummins KD, Shen F, Shan X, Veliz K, Blouch K, Yashiro-Ohtani Y, Kenderian SS, Kim MY, O'Connor RS, Wallace SR, Kozlowski MS, Marchione DM, Shestov

M, Garcia BA, June CH, Gill S, Human chimeric antigen receptor macrophages for cancer immunotherapy. Nat. Biotechnol. 38, 947–953 (2020). [PubMed: 32361713]

62. Mederacke I, Dapito DH, Affò S, Uchinami H, Schwabe RF, High-yield and high-purity isolation of hepatic stellate cells from normal and fibrotic mouse livers. Nat. Protoc. 10, 305–315 (2015). [PubMed: 25612230]

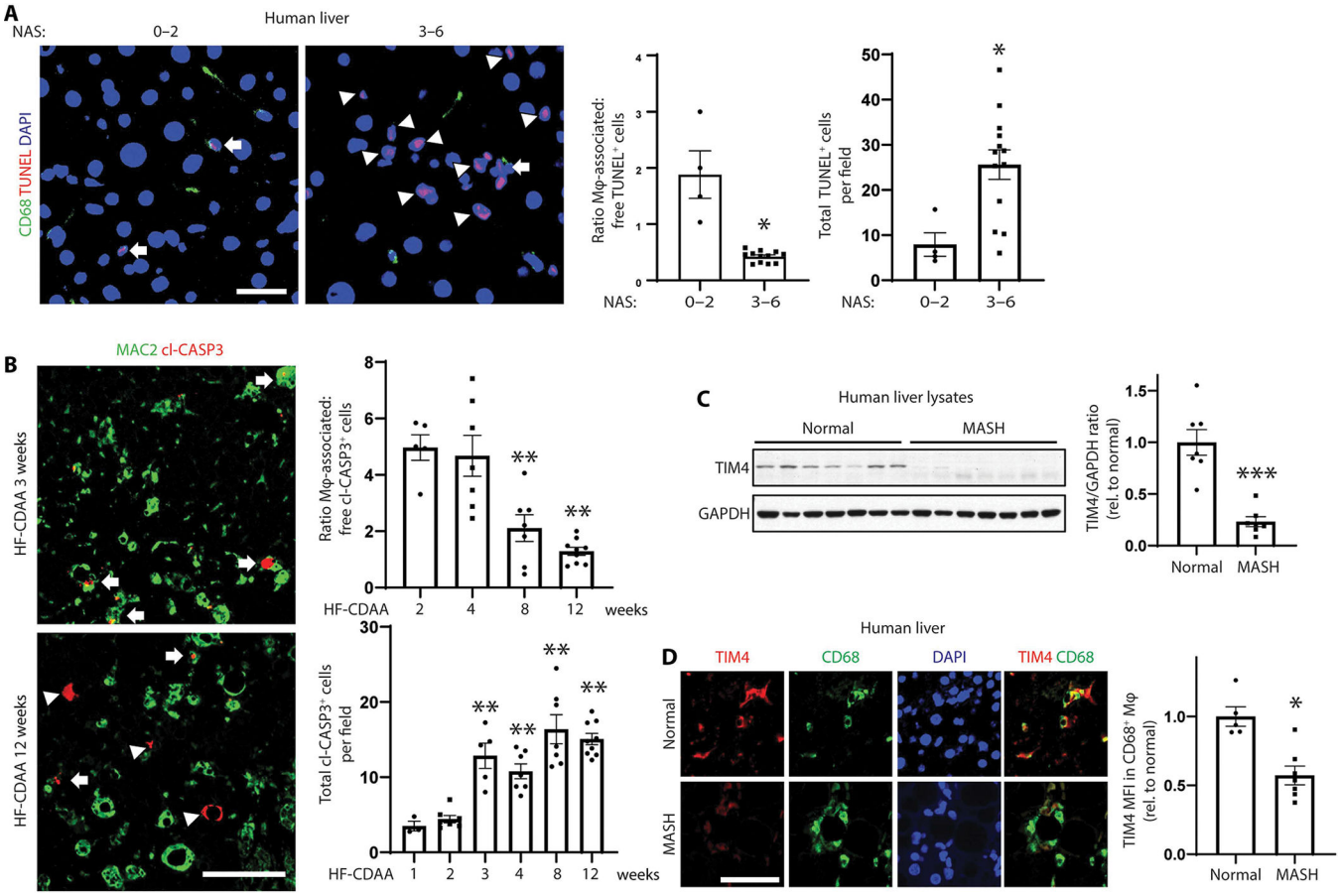

Fig. 1. Efferocytosis by liver macrophages and the efferocytosis receptor TIM4 are decreased in human and experimental steatohepatitis.

(**A**) Immunostaining of human liver sections from patients with a NAS of 0 to 2 or 3 to 6 using TUNEL (cell death) and anti-CD68 (macrophage, Mϕ) is shown on the left. Scale bar, 50 μm. Arrows indicate macrophage-associated TUNEL$^+$ cells, and arrowheads indicate macrophage-free TUNEL$^+$ cells. Efferocytosis was determined by calculating the ratio of macrophage-associated:free TUNEL$^+$ cells (middle graph) and total TUNEL$^+$ cells per field (right graph, $n = 4$ in the NAS 0 to 2 group and 13 in the NAS 3 to 6 group). (**B**) Livers from mice fed the HF-CDAA diet for the indicated weeks were assayed for efferocytosis, using anti–cleaved caspase3 (cl-CASP3, red) to mark apoptotic cells and anti-MAC2 (green) to stain macrophages ($n = 3$ to 9 mice per group). Examples of images at 3 and 12 weeks of diet feeding are shown on the left. Scale bar, 100 μm. Arrows indicate macrophage-associated apoptotic cells, and arrowheads indicate macrophage-free apoptotic cells. Quantification is shown in the graphs on the right. (**C**) Immunoblots (left) of TIM4 in another cohort of human normal and MASH liver, with data quantification (right, $n =$ 7 per group). Glyceraldehyde phosphate dehydrogenase (GAPDH) was used as the loading control, and the data were quantified by the ratio of TIM4 to GAPDH band density and then normalized to the normal group. (**D**) The human normal and MASH liver sections used in (A) were immunostained for TIM4 (red) and CD68 (green), shown on the left. Scale bar, 50 μm. Data were quantified (right) as TIM4 MFI in CD68$^+$ macrophages relative to normal

liver ($n = 5$ in the normal group, and $n = 7$ in the MASH group). For immunofluorescence images, nuclei are stained with 4′,6-diamidino-2-phenylindole (DA PI; blue). All data are means ± SEM. $*P < 0.05$, $**P < 0.01$, and $***P < 0.001$ by Student's *t* test [(A), (C), and (D)] or one-way ANOVA (B) followed by Fisher's LSD post hoc analysis.

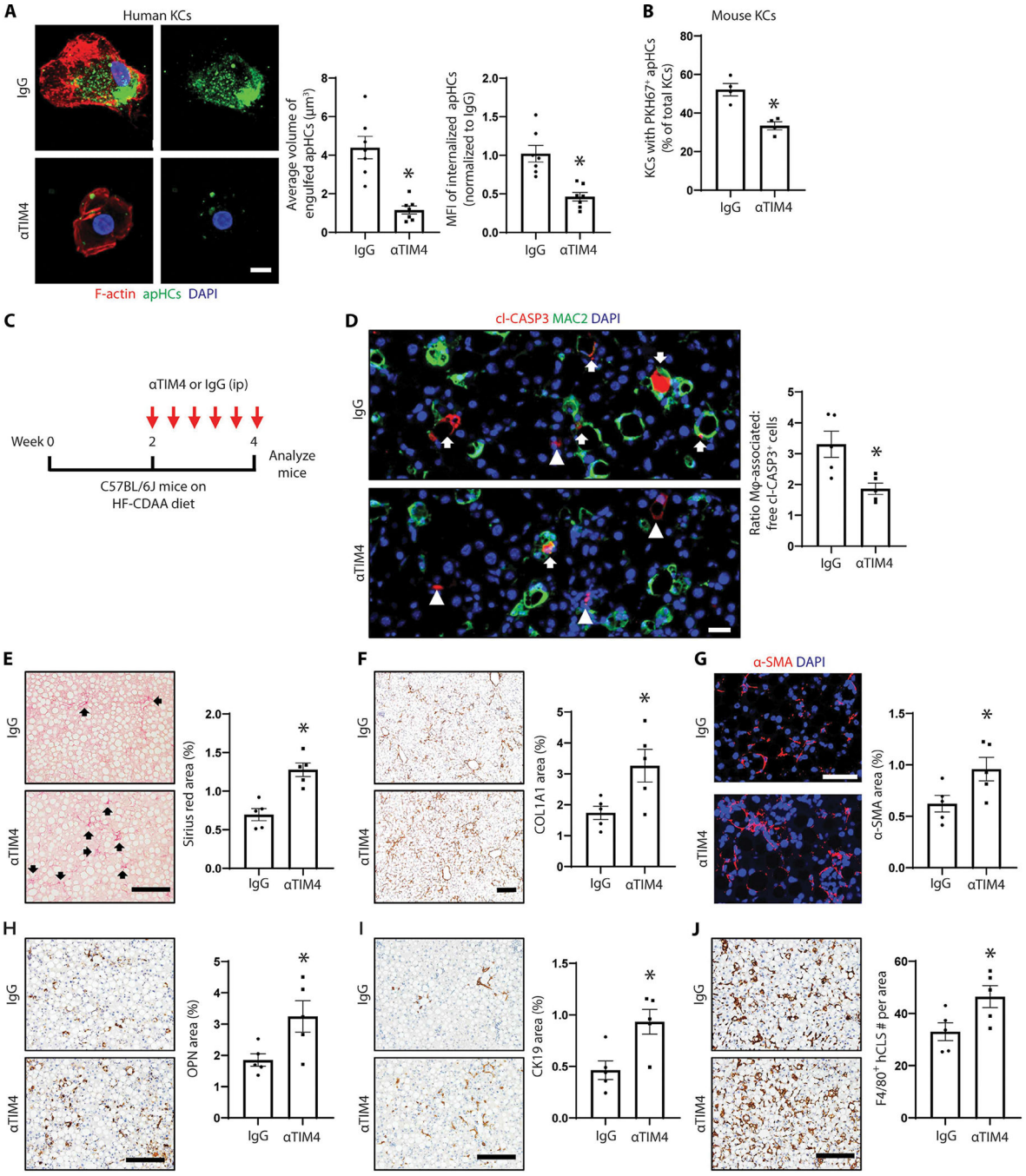

Fig. 2. Anti-TIM4 reduces efferocytosis and accelerates liver fibrosis in experimental steatohepatitis.

(**A**) Images (left) of primary human KCs stained for F-actin (red) after exposure to apoptotic human hepatocytes (apHCs; green) for 6 hours in the presence of IgG or anti-TIM4. Scale bar, 10 μm. The data were quantified (right) as both the average volume of engulfed cargo and the MFI of internalized apHCs ($n = 7$ biological replicates per group). (**B**) Quantification of efferocytosis by primary mouse KCs after exposure to PKH67-labeled apoptotic mouse hepatocytes ($n = 4$ biological replicates per group). (**C**) Schematic

experimental design showing how mice were fed the HF-CDAA MASH diet for 4 weeks and treated with IgG or anti-TIM4 during weeks 3 to 4 ($n = 5$ mice per group). ip, intraperitoneal. (**D**) Images (left) of liver sections immunostained with anti-MAC 2 (green) and anti–cl-CA SP3 (red). Scale bar, 25 μm. Arrows depict efferocytic macrophages, and arrowheads depict macrophage-free apoptotic cells. Efferocytosis was quantified (right) as in Fig. 1B. (**E**) Staining (left) and quantification (right) of Sirius red–positive area. Scale bar, 200 μm. (**F**) Immunostaining (left) and quantification (right) of COL 1A1-positive area. Scale bar, 200 μm. (**G**) Immunostaining (left) and quantification (right) of α-SMA–positive area (red). Scale bar, 50 μm. (**H**) Immunostaining (left) and quantification (right) of OPN-positive area. Scale bar, 200 μm. (**I**) Immunostaining (left) and quantification (right) of CK19-positive area. Scale bar, 200 μm. (**J**) Immunostaining (left) of F4/80, with quantification (right) of $F4/80^+$ hCLS/area. Scale bar, 200 μm. For immunofluorescence images, nuclei are stained with DA PI (blue). All data are means ± SEM. $*P < 0.05$ by Student's *t* test.

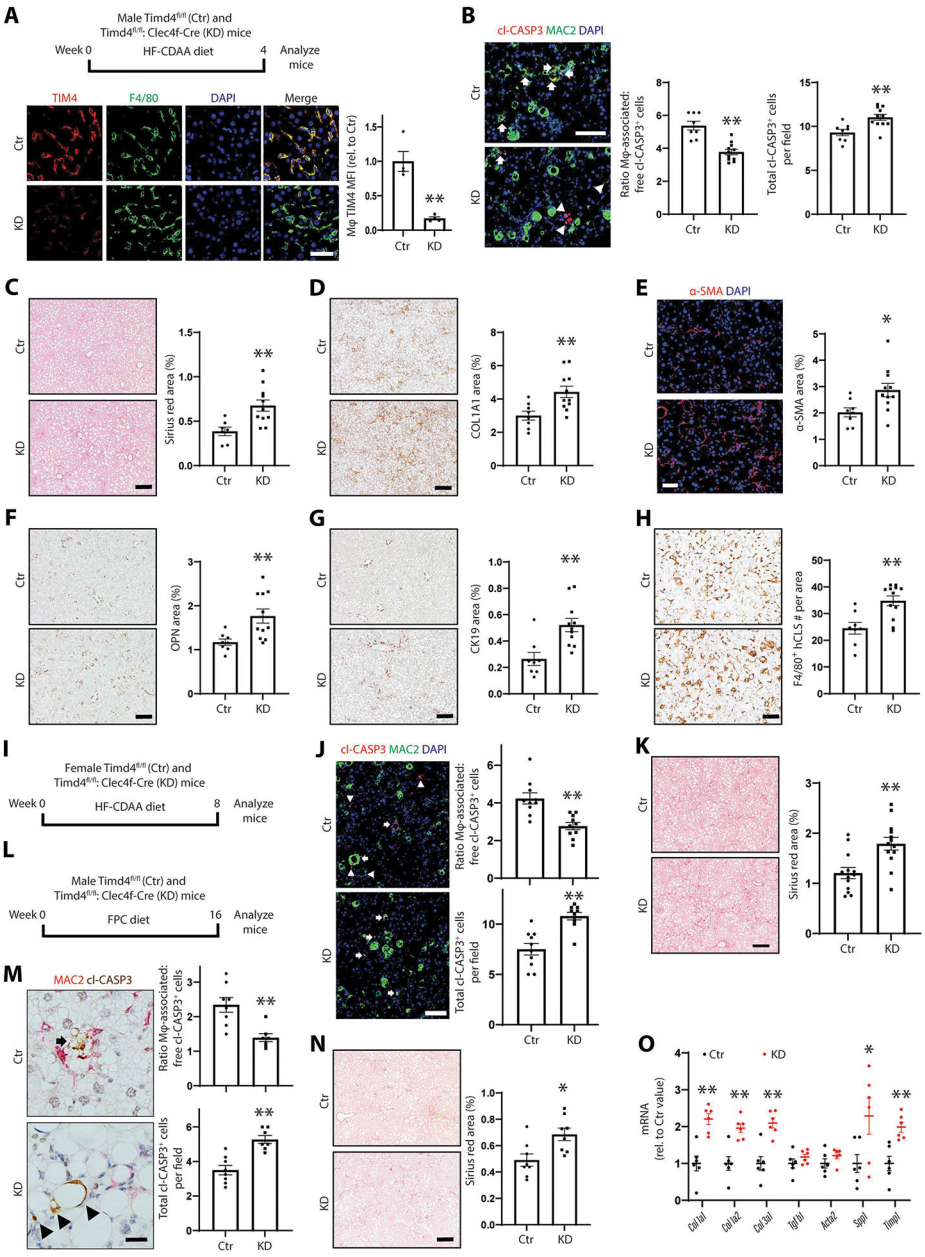

Fig. 3. KD of KC TIM4 decreases efferocytosis and accelerates liver fibrosis in HF-CDAA diet–induced steatohepatitis.

(**A** to **H**) *Timd4*$^{fl/fl}$ (control, Ctr) and *Timd4*$^{fl/fl}$;*Clec4f-Cre*$^{+/-}$ (KD) male mice were fed the HF-CDAA diet for 4 weeks (n = 8 to 10 mice per group). (A) Schematic experimental design and efficiency of KC TIM4 KD as assessed through immunostaining (left) of liver sections using anti-TIM4 (red) and anti-F4/80 (green). Data were quantified (right) as macrophage TIM4 MFI relative to control mice (n = 4 mice per group). Scale bar, 50 μm. (B) Images (left) of liver sections immunostained with anti-MAC2 (green) and anti–cl-CA SP3 (red). Scale bar, 50 μm. Arrows depict efferocytic macrophages, and arrowheads depict macrophage-free apoptotic cells. Efferocytosis was quantified as in Fig. 1A. (C) Staining (left) and quantification (right) of Sirius red–positive area. Scale bar, 200 μm.

(D) Immunostaining (left) and quantification (right) of COL 1A1-positive area. Scale bar, 200 μm. (E) Immunostaining (left) and quantification (right) of α-SMA–positive area (red). Scale bar, 50 μm. (F) Immunostaining (left) and quantification (right) of OPN-positive area. Scale bar, 200 μm. (G) Immunostaining (left) and quantification (right) of CK19-positive area. Scale bar, 200 μm. (H) Immunostaining (left) of F4/80, with quantification (right) of hCLS/area. Scale bar, 200 μm. (**I** to **K**) *Timd4*$^{fl/fl}$ (control, Ctr) and *Timd4*$^{fl/fl}$;*Clec4f-Cre*$^{+/-}$ (KD) female mice were fed the HF-CDAA diet for 8 weeks (n = 13 mice per group). (I) Schematic experimental design. (J) Images (left) of liver sections immunostained with anti-MAC2 (green) and anti–cl-CASP3 (red). Scale bar, 100 μm. The arrows depict an efferocytic macrophage, and the arrowheads depict macrophage-free apoptotic cells. Efferocytosis was quantified (right) as in Fig. 1A. (K) Staining (left) and quantification (right) of Sirius red–positive area. Scale bar, 200 μm. (**L** to **O**) *Timd4*$^{fl/fl}$ (control, Ctr) and *Timd4*$^{fl/fl}$; *Clec4f-Cre* (KD) male mice were fed the FPC diet for 16 weeks (n = 8 or 9 mice per group). (L) Schematic experimental design. (M) Images (left) of liver sections immunostained with anti-MAC 2 (red) and anti–cl-CASP3 (brown). Scale bar, 50 μm. The arrow depicts an efferocytic macrophage, and the arrowheads depict macrophage-free apoptotic cells. Efferocytosis was quantified (right) as in Fig. 1A. (N) Staining (left) and quantification (right) of Sirius red–positive area (arrows). Scale bar, 200 μm. (O) Liver mRNAs for the indicated fibrogenic genes expressed relative to the values for control mice. For immunofluorescence images, nuclei are stained with DA PI (blue). All data are means ± SEM. *P < 0.05 and **P < 0.01 by Student's t test.

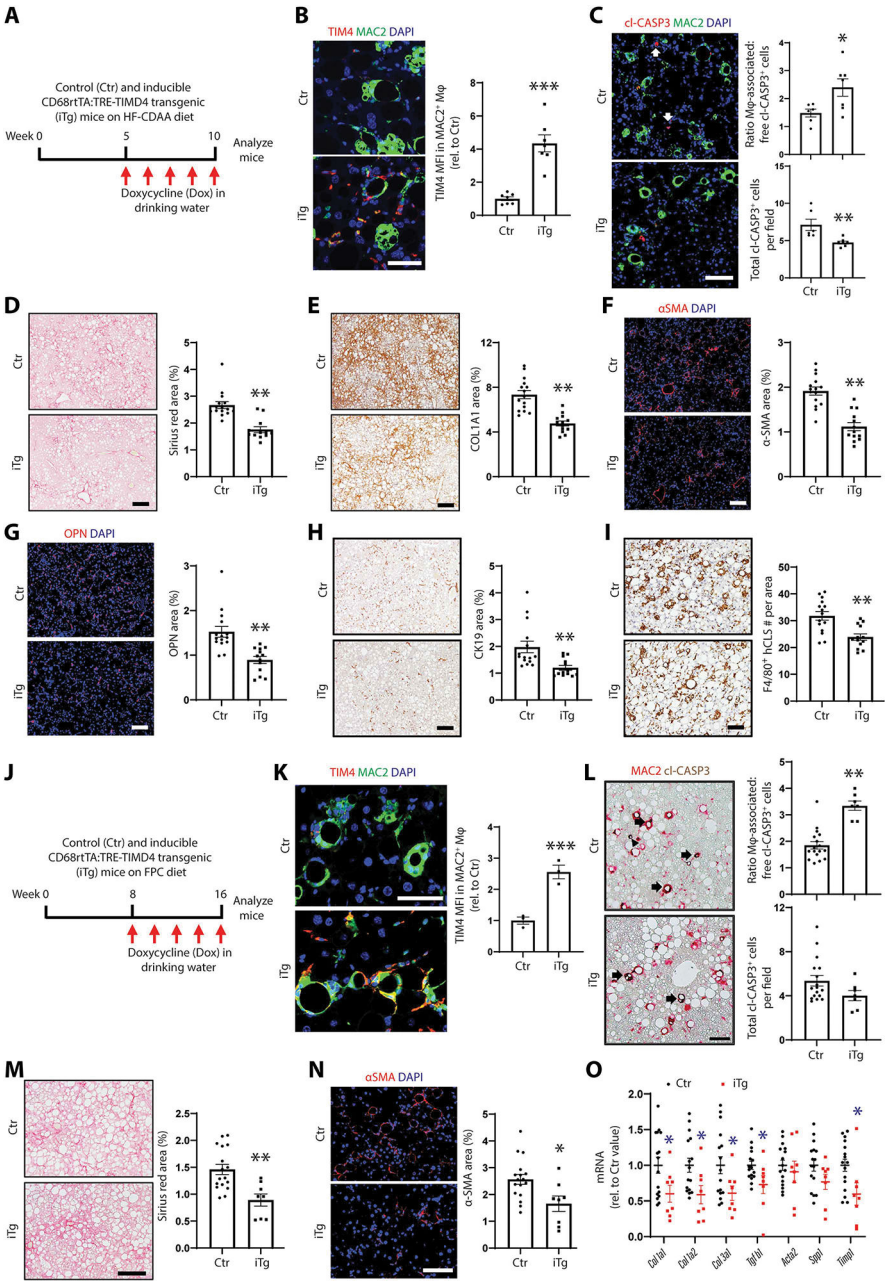

Fig. 4. TIM4 restoration in liver macrophages in HF-CDAA and FPC diet–induced steatohepatitis/MASH promotes efferocytosis and lowers liver fibrosis.

(**A**) Schematic experimental design using control mice (TRE-TIMD4 and CD68rtTA; Ctr; $n = 15$) and inducible CD68rtTA:TRE-TIMD4 transgenic mice (iTg, $n = 13$) fed the HF-CDAA diet for 10 weeks, with Dox (75 μg/ml) added to the drinking water during weeks 6 to 10. (**B**) Immunostaining (left) of liver sections using anti-TIM4 (red) and anti-MAC 2 (green). Data were quantified (right) as macrophage TIM4 MFI relative to control mice. Scale bar, 50 μm. (**C**) Images (left) of liver sections immunostained with anti-MAC 2 (green) and anti–cl-CASP3 (red). Scale bar, 25 μm. Arrows depict macrophage-free apoptotic cells. Efferocytosis was quantified (right) as in Fig. 1A. (**D**)

Staining (left) and quantification (right) of Sirius red–positive area. Scale bar, 200 μm. (**E**) Immunostaining (left) and quantification (right) of COL 1A1-positive area. Scale bar, 200 μm. (**F**) Immunostaining (left) and quantification (right) of α-SMA–positive area (red). Scale bar, 100 μm. (**G**) Immunostaining (left) and quantification (right) of OPN-positive area (red). Scale bar, 100 μm. (**H**) Immunostaining (left) and quantification (right) of CK19-positive area. Scale bar, 200 μm. (**I**) Immunostaining (left) of F4/80, with quantification (right) of hCLS/area. Scale bar, 200 μm. (**J**) Schematic experimental design using control mice (TRE-TIMD4 and CD68rtTA; Ctr; $n = 17$) and inducible CD68rtTA:TRE-TIMD4 transgenic mice (iTg, $n = 8$) fed the FPC diet for 16 weeks, with Dox (50 μg/ml) added to the drinking water during weeks 9 to 16. (**K**) Immunostaining (left) of liver sections using anti-TIM4 (red) and anti-MAC 2 (green). Data were quantified (right) as macrophage TIM4 MFI relative to control mice ($n = 3$ mice per group). Scale bar, 50 μm. (**L**) Images (left) of liver sections immunostained with anti-MAC 2 (red) and anti–cl-CA SP3 (brown). Scale bar, 100 μm. Arrows depict efferocytic macrophages, and the arrowhead depicts a macrophage-free apoptotic cell. Efferocytosis was quantified (right) as in Fig. 1A. (**M**) Staining (left) and quantification (right) of Sirius red–positive area. Scale bar, 100 μm. (**N**) Immunostaining (left) and quantification (right) of α-SMA–positive area (red). Scale bar, 50 μm. (**O**) Liver mRNAs for the indicated fibrogenic genes, expressed relative to the values for control mice. All data are means ± SEM. $*P < 0.05$, $**P < 0.01$, and $***P < 0.001$ by Student's *t* test.

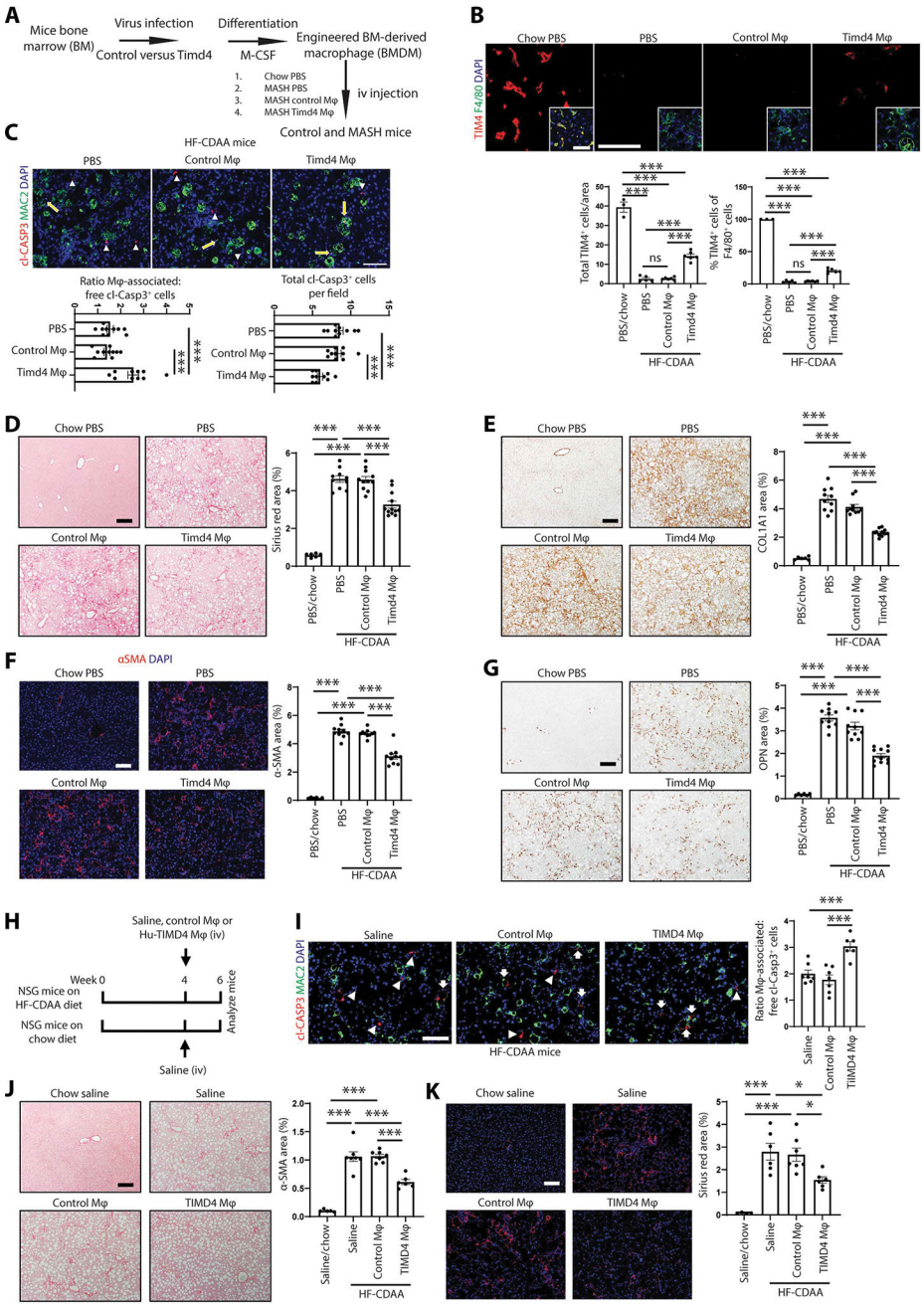

Fig. 5. Treating steatohepatitis mice with TIM4-expressing macrophages promotes efferocytosis and lowers liver fibrosis.

(**A** to **G**) C57BL/6J mice fed the HF-CDAA diet for 16 weeks were intravenously (iv) injected biweekly with PBS (vehicle control) (n = 10 mice), control (Ctrl) BMDMs (n = 11 mice), or BMDMS transduced with retroviral *Timd4* (Timd4-BMDMs, n = 12 mice). A fourth group of mice was maintained on a chow diet for the duration of the experiment and injected with PBS vehicle (n = 6 mice). The livers were harvested for analysis 2 weeks later. (A) Schematic exerimental design. M-CSF, macrophage colony-stimulating factor. (B) Staining (top) and quantification (bottom) of livers for TIM4 expression per area and per total F4/80+ macrophages. Scale bar, 50 μm. (C) Images

(top) of liver sections immunostained with anti-MAC2 (green) and anti–cl-CASP3 (red). Scale bar, 100 μm. Arrows depict efferocytic macrophages, and arrowheads depict a macrophage-free apoptotic cell. Efferocytosis was quantified (bottom) as in Fig. 1A. (D) Staining (left) and quantification (right) of Sirius red–positive area. Scale bar, 200 μm. (E) Immunostaining (left) and quantification (right) of COL 1A1-positive area. Scale bar, 200 μm. (F) Immunostaining (left) and quantification (right) of α-SMA–positive area (red). Scale bar, 50 μm. (G) Immunostaining (left) and quantification (right) of OPN-positive area. Scale bar, 200 μm. (**H** to **K**) NSG mice fed the HF-CDAA diet for 4 weeks were injected intravenously with saline vehicle ($n = 7$ mice), control HMDMs ($n = 7$ mice), or HMDMs differentiated from monocytes transduced with retrovirus encoding *TIMD4* (TIMD4 HMDMs; $n = 6$ mice). A fourth group of mice was maintained on a chow diet for the duration of the experiment and injected with saline vehicle ($n = 5$ mice). The livers were harvested for analysis 2 weeks later. (H) Schematic experimental design. (**I**) Images (left) of liver sections immunostained with anti-MAC 2 (green) and anti–cl-CA SP3 (red). Scale bar, 100 μm. Arrows depict efferocytic macrophages, and arrowheads depict macrophage-free apoptotic cells. Efferocytosis was quantified (right) as in Fig. 1A. (J) Staining (left) and quantification (right) of Sirius red–positive area. Scale bar, 200 μm. (K) Immunostaining (left) and quantification (right) of α-SMA–positive area (red). Scale bar, 50 μm. All data are means ± SEM. $*P < 0.05$ and $***P < 0.001$ for all panels by one-way ANOVA followed by Fisher's LSD post hoc analysis.

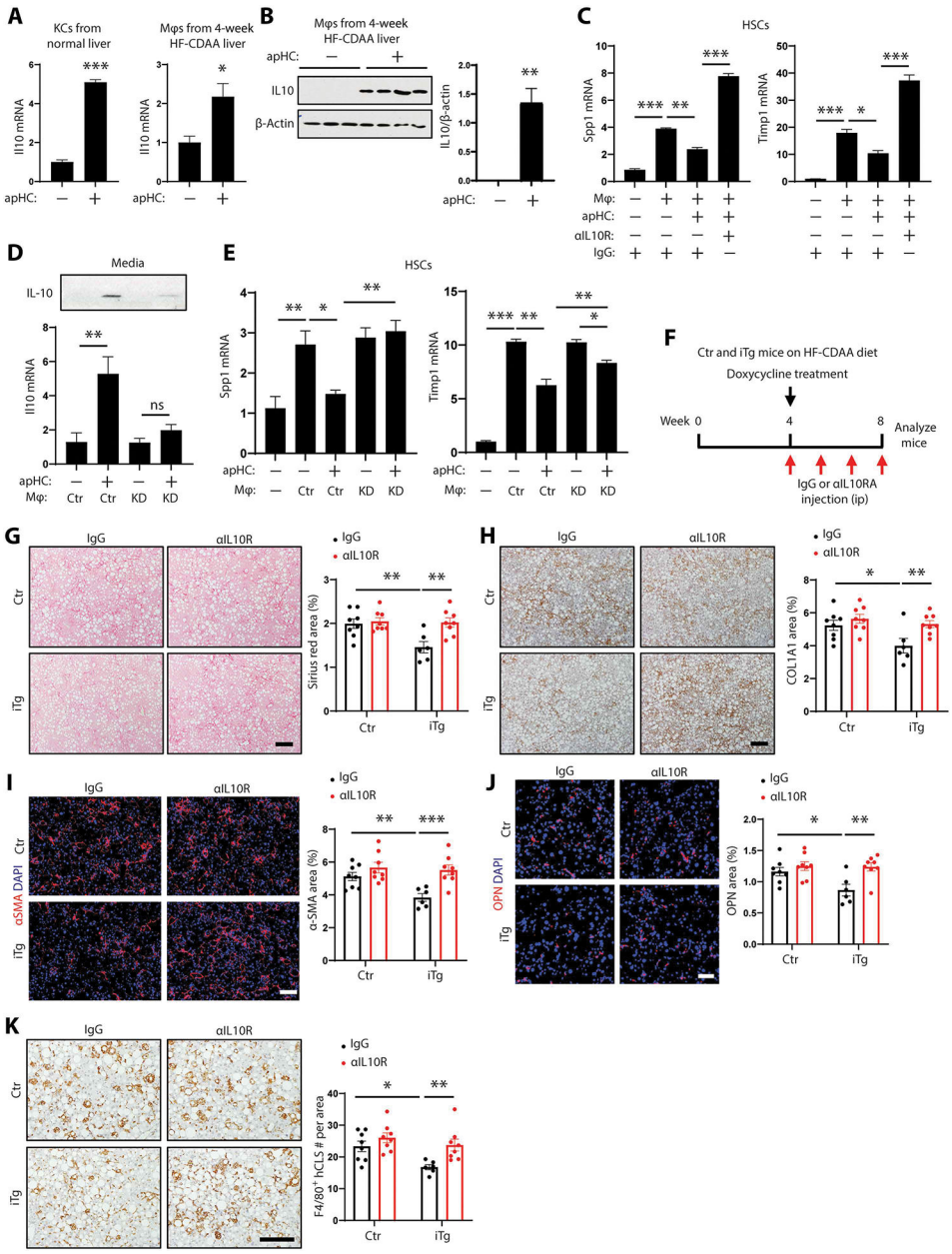

Fig. 6. Evidence that IL-10 secreted by efferocytosing TIM4+ macrophages lowers HSC activation and liver fibrosis in steatohepatitis.

(**A**) *IL10* expression in primary mouse KCs (left) and liver macrophages (right) from 4-week HF-CDAA mice (early steatohepatitis) incubated with or without apHCs ($n = 3$ or 4 biological replicates per group) The mRNA data were normalized to unfed control KCs or early steatohepatitis macrophages. (**B**) Immunoblot of IL-10 (left) with quantification (right) in early steatohepatitis macrophages incubated with or without apHCs. β-Actin was used as the loading control, and the data were quantified by the ratio of IL-10 to β-actin. (**C**) CM was collected from macrophages incubated with or without apHCs and then transferred to primary mouse HSCs treated with TGF-β1 (5 ng/ml) with or without anti–IL-10R antibody or control IgG antibody. After 48 hours, the HSCs were assayed for *Spp1* (left) and *Timp1*

(right) mRNA expression (n = 4 biological replicates per group). (**D**) Macrophages isolated from 4-week HF-CDAA–fed control (Ctr) or TIM4-KD mice (see Fig. 2) were incubated with or without apHCs. IL-10 protein in the medium was assayed by immunoblot (top), and *Il10* mRNA in the cells was assayed by quantitative polymerase chain reaction (qPCR; bottom, n = 4 biological replicates per group). (**E**) The CM from the experiment in (D) was transferred to TGF-β1–activated primary mouse HSCs and assayed 48 hours later for *Spp1* (left) and *Timp1* (right) mRNAs. (**F**) Schematic experimental design. Control mice (TRE-TIMD4 and CD68rtTA; Ctr) and inducible CD68rtTA:TRE-TIMD4 transgenic mice (iTg) were fed the HF-CDAA diet for 8 weeks. During weeks 5 to 8, Dox (75 μg/ml) was added to the drinking water, and the mice were injected intraperitoneally (three times/week) with 200 μg per mouse anti–IL-10R or IgG antibody (n = 8, 8, 6, and 8 mice per group). (**G**) Staining (left) and quantification (right) of Sirius red–positive area. Scale bar, 200 μm. (**H**) Immunostaining (left) and quantification (right) of COL 1A1-positive area. Scale bar, 200 μm. (**I**) Immunostaining (left) and quantification (right) of α-SMA–positive area (red). Scale bar, 100 μm. (**J**) Immunostaining (left) and quantification (right) of OPN-positive area (red). Scale bar, 50 μm. (**K**) Immunostaining (left) of F4/80, with quantification (right) of hCLS/area. Scale bar, 200 μm. All data are means ± SEM. *P < 0.05, **P < 0.01, and ***P < 0.001 by Student's t test for (A) and (B), by one-way ANOVA for (C) to (E) followed by Fisher's LSD post hoc analysis, and by two-way ANOVA for (G) to (K) followed by Fisher's LSD post hoc analysis.